



Cite this: *Sustainable Energy Fuels*, 2025, 9, 4959

Toward sustainable fuel formulations: thermophysical assessment of a synthetic oxygenated blend formed from hexane + cyclopentyl methyl ether + propan-1-ol†

Isaías Huenuvil-Pacheco, Marcela Cartes and Andrés Mejía *

This study provides a comprehensive thermophysical characterization of a new potential oxygenate fuel composed of hexane as a surrogate for fossil fuel, cyclopentyl methyl ether (CPME) as a synthetic fuel, and propan-1-ol as a biofuel. The thermophysical characterization of this ternary mixture is based on the main thermophysical properties involved in the gasoline formulation and evaluation, namely the vapor-liquid equilibria (VLE) at 94 kPa from 338 to 365 K, the liquid mass density, the liquid viscosity, and the surface tension at 298.15 K and 101.3 kPa. All thermophysical properties are measured in the whole mole fraction range. These experimental data are accurately and fully predicted using the SAFT-VR Mie EoS coupled with Helmholtz scaling theory and square gradient theory. The advantage of this theoretical approach is the prediction of the related properties in a broad range of temperature, pressure, and mole fractions needed for the use of oxygenated gasoline, which according to industrial applications are 298.15 K to 314.15 K, 70 to 120 kPa, and 80% v/v hydrocarbons, 5–20% v/v octane number enhancement, respectively. According to the results, the mixture is zeotropic with a positive deviation from Raoult's law, while the liquid mass density, the liquid viscosity, and the surface tension show negative deviations from the ideal behavior. Complementarily, the interfacial theory reveals that CPME does not exhibit surface activity; propan-1-ol adsorbs at high hexane concentration and hexane adsorbs at low hexane concentration.

Received 28th May 2025

Accepted 22nd July 2025

DOI: 10.1039/d5se00759c

rsc.li/sustainable-energy

1 Introduction

The modern world relies on energy in various forms for its daily activities, and its demand is continuously rising, driven by factors such as population growth and rapid technological advancements.^{1,2} Currently, most energy is derived from non-renewable fossil fuels, which are widely used across sectors like industry, agriculture, and transportation. However, the combustion of these fuels is the primary source of emissions of pollutants such as carbon dioxide (CO₂), nitrogen oxides (NO_x), and other environmentally harmful gases.³ The transportation sector accounts for approximately 23% of global CO₂ emissions, making it a significant contributor to pollution.⁴ Considering the increasingly stringent emission regulations and the finite availability of fossil fuels, it is essential to promote the development of eco-friendly and renewable fuel alternatives,^{2,5} such as oxygenated fuels based on biofuels and synthetic fuels. The

most common oxygenates in commercial gasoline are primary alcohols (e.g., methanol, ethanol, propanol and butanol and their isomers) and ethers (e.g., diisopropyl ether (DIPE), ethyl *tert*-butyl ether (ETBE), methyl *tert*-butyl ether (MTBE), *tert*-amyl methyl ether (TAME), and *tert*-amyl ethyl ether (TAEE)) which display blending properties, such as Research Octane Number (RON), Motor Octane Number (MON), Reid Vapor Pressure (RVP), and stoichiometric air/fuel, similar to gasoline, as can be seen in Table 1.

These oxygenated additives are blended in 5 to 20% v/v with fuel to increase the octane rating of the fuel,^{6–8,11} decreasing harmful gas emissions from spark-ignited engines, as well as reducing the fraction of unburned hydrocarbons released into the atmosphere.^{12–15}

Notwithstanding similar blending properties, the use of some of these oxygenated compounds has decreased because they present disadvantages. For example, some alcohols increase pollutant gas emissions, while some ethers present a high degree of toxicity to human life.¹⁴ Considering the positive effects of oxygenates on fuels and their side effects, it is necessary to find better alternatives in the formulation of fuel blends, which need to focus on the correct balance between environmentally friendly and efficient gasoline blends.

Departamento de Ingeniería Química, Universidad de Concepción, POB 160-C, Correo 3, Concepción, Bío-Bío, Chile. E-mail: amejia@udec.cl; Tel: +56 412203897

† Electronic supplementary information (ESI) available. Experimental determination and theoretical modeling of the liquid viscosity of the CPME (2) + propan-1-ol binary mixture at 298.15 K and 101.30 kPa. See DOI: <https://doi.org/10.1039/d5se00759c>



Table 1 Selected blending properties of gasoline and oxygenates for gasoline^a

Component	RON	MON	RVP (kPa)	Stoichiometric air/fuel
Gasoline	96.8	81–89	55–103	14.70
Methanol	133.0	99.0	414	6.40
Ethanol	108.6	89.7	117.3	8.95
Propan-1-ol	118.0	98.0	6.20	10.35
Propan-2-ol	121.0	96.0	96.6	10.40
<i>i</i> -Butanol	105.0	92.0	34.5	11.10
<i>n</i> -Butanol	94.0	81.0	44.2	11.20
<i>t</i> -Butanol	109.0	93.0	60.7	11.12
CPME	115–118	—	8.83	12.41
DIPE	110.0	99.0	33.8	12.10
ETBE	119.0	103.0	27.6	12.20
MTBE	117.0	102.0	55.2	11.70
TAME	110.0	99.0	10.4	12.10
TAEE	118.0	95.0	33.8	14.50

^a The numerical values were taken from Luque and Clark,⁶ Elvers and Schütze,⁷ and Nanda *et al.*⁸ except for cyclopentyl methyl ether (CPME) whose values were taken from de Gonzalo *et al.*⁹ and Watanabe *et al.*¹⁰

Attractive alternatives include formulating renewable oxygenated fuels, where bio-alcohols and renewable ethers can be used as blending agents in reformulating petroleum-derived gasoline.^{12,16}

Bio-alcohols, such as bioethanol, biopropanol, and biobutanol, may have acceptable properties as gasoline blending components (see Table 1) and are also considered potential second-generation biofuels because they can be produced from biomass resources, which represent a possibly inexhaustible source of feedstock for biofuel production.^{17,18} The presence of bioalcohol as an additive to fossil fuels decreases nitrogen oxides (NO_x) and particulate matter (PM) because the alcohol provides more oxygen and high latent heat during combustion. On the other hand, these alcohols promise to be a solution to incomplete combustion, serving as fuel additives that improve the air-fuel ratio by providing additional oxygen.¹⁹ In addition to the above, it highlights its renewable, agricultural feedstock procurement, reducing dependence on fossil resources.²⁰ According to Luque and Clark,⁶ Elvers and Schütze,⁷ and Nanda *et al.*⁸ bioethanol has been traditionally used as fuel or oxygenate additive, while biobutanol has been shown to have superior properties as an oxygenate to bioethanol,^{6,8} with lower solubility in water. Recently, biopropanol has been positioned as a future biofuel due to its blending properties (*i.e.*, RON and MON values higher than those for ethanol and butanol, but notorious lower RVP – see Table 1), its versatility for use in gasoline^{21,22} and diesel^{23–25} with high-performance metrics in engine test and lower exhaust emissions.

In the case of ethers, there is a need for new alternatives that are more environmentally friendly and less polluting. In this regard, cyclopentyl methyl ether (CPME) has emerged as a promising candidate, owing to its favorable technical blending properties (*e.g.*, higher RON and lower RVP than other ethers, see Table 1 and its references) and environmental properties. Thus, CPME is a solvent characterized by a high boiling point (106 °C), low water solubility (1.1 g CPME/100 g

H₂O), easy separation and recovery of water, and low peroxide formation rate, among other properties. From a toxicological point of view, this ether shows a mild level of toxicity with moderate irritation, with negative genotoxicity and mutagenicity.^{9,10}

Based on the technical, environmental, and renewability considerations, new gasoline blends will be formulated with bio-based and renewable oxygenates, such as bio-alcohol (*e.g.*, bio-ethanol, bio-propanol, or bio-butanol) and cyclopentyl methyl ether. In order to consider these compounds as potential oxygenated additives, it is necessary to carry out several development levels or steps, where the main steps include:⁷ evaluation of thermophysical properties of the blends (*e.g.*, hydrocarbons + renewable ether + bio-alcohol), engine laboratory tests, toxicity and environmental evaluations, fuel stability, cleanliness, safety, among others.

Considering the first stage, it is essential to accurately describe selected thermophysical properties of the blends (*e.g.*, hydrocarbons + renewable ether + bio-alcohol) in a broad range of composition, as a function of temperature and pressure, including fluid phase equilibrium, liquid mass density, transport, and surface properties. In particular, vapor–liquid equilibrium is of great importance in estimating the Reid vapor pressure (RVP), which is a key indicator to assess compliance with environmental and performance regulations, such as vapor lock, percolation, fuel vaporization, and pollutant emissions.²⁶ On the other hand, the magnitude of liquid mass density, liquid viscosity, and surface tension plays a key role in gasoline performance, which affects the fuel atomization process in the cylinder of diesel engines, controlling parameters such as combustion level and emissions generated by the engine.²⁷

In previous studies, we explored the behavior of selected thermophysical properties involved in the evaluation of oxygenate fuel blends (*i.e.*, phase equilibria, liquid mass density, liquid viscosity, and surface tension) of two surrogate oxygenated gasoline blends formed from *n*-hexane + cyclopentyl methyl ether + ethanol^{28,29} and *n*-hexane + cyclopentyl methyl ether + butan-1-ol ternary mixtures,³⁰ as well as the corresponding binary mixtures formed from cyclopentyl methyl ether, namely cyclopentyl methyl ether + ethanol mixture,³¹ cyclopentyl methyl ether + *n*-hexane mixture,³² cyclopentyl methyl ether + butan-1-ol mixture,³³ and cyclopentyl methyl ether + propan-1-ol mixture.³⁴ From these studies, it is possible to observe that the vapor–liquid equilibria of the ternary mixtures and the associated binary mixtures of cyclopentyl methyl ether binary mixtures display a positive deviation from Raoult's law, and also the binary mixtures formed from cyclopentyl methyl ether with propan-1-ol and butan-1-ol exhibit azeotropic behavior. The liquid mass density, liquid viscosity, and surface tension of the ternary mixtures display a monotonic behavior with the liquid mole fraction and exhibit a negative deviation from the linear dependence on the mole fraction. Similar behavior is found for the cyclopentyl methyl ether binary mixtures, except for the cases of the cyclopentyl methyl ether + propan-1-ol or butan-1-ol binary mixtures, where the surface tension displays a positive deviation. The described



behavior of these thermophysical properties was also confirmed by thermodynamic modeling, where cubic and molecular-based equations of state (EoSs) were applied to model the phase equilibria and liquid mass densities. Furthermore, these EoSs were coupled with the free-volume theory^{35,36} to describe the liquid viscosities and with the square gradient theory³⁷⁻³⁹ to predict their interfacial properties, including the concentration distribution along the interfacial region and surface tensions of the mixtures.

Based on these previous studies oriented towards the characterization of cyclopentyl methyl ether as a potential renewable and eco-friendly oxygenate, and considering the new findings and promising uses of propan-1-ol as an oxygenated additive (*e.g.*, low emissions and a higher octane number),^{6-8,22-25,40} we propose a new and unexplored surrogate oxygenated gasoline blend formed from *n*-hexane, cyclopentyl methyl ether, and propan-1-ol, which represents a potential and interesting mixture for application to gasoline blends, with the necessary characteristics to contribute to the resolution of environmental problems but considering the technical aspects (see Table 1).

Specifically, this work reports the isobaric vapor–liquid equilibrium data at 94 kPa, the liquid mass density, the liquid viscosity and the surface tension data at 101.3 kPa and 298.15 K, together with a full predictive theoretical framework based on the statistical association fluid theory (SAFT), where the fluid interactions are described by a variable-range Mie potential, SAFT-VR Mie EoS,⁴¹ coupled with the Helmholtz scaling (A-scaling) theory,⁴² and with the van der Waals square gradient theory.³⁷⁻³⁹ It is worth mentioning that the principal advantage of the models used here is that they allow the full prediction of the thermophysical properties of the ternary system only using information from the pure fluids and the constitutive binary mixtures.

2 Experimental section

2.1 Materials

Cyclopentyl methyl ether (CPME) was supplied by Sigma-Aldrich, while *n*-hexane and propan-1-ol were obtained from Merck. These chemicals were used directly without additional purification methods. Table 2 presents the purity specifications provided by the manufacturer, along with our verifications using gas chromatography (GC) which are based on a Varian 3400 GC provided with a thermal conductivity detector and a Thermo Separation Products model SP4400 electronic integrator, and using a separation column (3 m long and 0.3 cm in diameter), packed with SE-30. The GC conditions were 473.15 K

for the column, 483.15 K for the injector, and 493.15 K for the detector. The GC test confirms and verifies the purity of the chemical components as indicated by the manufacturer. Table 2 also includes the water content of these three chemicals measured using a Karl Fischer device.

In addition to Table 2, the purity and quality of the fluids used here have been validated by direct determination of the selected properties (*i.e.*, the normal boiling points at 101.3 kPa, the liquid mass densities, the liquid viscosities, and the surface tensions at 298.15 K and 101.3 kPa) utilizing the same devices used herein and allowing their application for experimental purposes.^{30,31,34}

2.2 Phase equilibria determination

For the isobaric vapor–liquid equilibrium (VLE) determination of the ternary mixture, a commercial all-glass vapor–liquid equilibrium apparatus (Fischer Labor and Verfahrenstechnik cell model 601, Germany) was used. In this Guillestre cell type, the equilibrium temperature was measured using a digital temperature meter (a Systemteknik model S1224) with a Pt 100 Ω probe with a precision estimated at ± 0.02 K. The pressure is measured and controlled with a Fischer pressure transducer with an overall accuracy estimated at ± 0.03 kPa. The concentrations (*i.e.*, liquid and vapor mole fractions) were measured using the variant GC, where the chromatography areas are converted to mole fractions using a calibration curve that guarantees an accuracy better than 0.001. The calibration of the temperature and the pressure devices and the experimental procedures used to measure the isobaric vapor–liquid equilibrium have been broadly described in our previous studies related to the measurement of VLE in binary and ternary mixtures that involve cyclopentyl methyl ether, *n*-hexane, or propan-1-ol.^{28,30-34,43}

2.3 Liquid mass density and liquid viscosity measurements

The liquid mass densities and the liquid viscosities for the ternary mixture are measured at 298.15 K and 101.3 kPa using a Stabinger viscometer (Anton Paar SVM 3001 M, Austria). This device is composed of two chambers that contain a vibrating U-tube, which is used to measure the liquid mass density, and two concentric cylinders where the internal cylinder rotates at a constant speed, and using the Couette principle, the liquid viscosity is measured. The instrument uncertainties are $\pm 5 \times 10^{-3}$ kg m⁻³ and $\pm 3.5 \times 10^{-3}$ mPa s, respectively. In this device, the isothermal condition is achieved with an internal bath within ± 0.01 K. The calibration of the densimeter and the

Table 2 Technical information of the pure fluids

Name	CAS	Supplier	Mass fraction purity (stated by the supplier)	Purification method	Mass fraction purity (detected with GC)	Water content mass fraction ^a
CPME	5614-37-9	Sigma-Aldrich	0.999	None	0.99	7.210×10^{-5}
<i>n</i> -Hexane	110-54-3	Merck	>0.998	None	0.99	3.660×10^{-5}
Propan-1-ol	71-23-8	Merck	>0.999	None	0.99	3.998×10^{-4}

^a Karl Fischer titration maximum relative uncertainty $u_r(w(H_2O)) = u(w(H_2O)/|w(H_2O)|)$ is 0.0173.



viscosimeter, as well as the experimental methodologies used here to determine the liquid mass density and liquid viscosity, has recently been described for measuring mixtures formed from cyclopentyl methyl ether, or *n*-hexane, or propan-1-ol.^{29,30,43}

2.4 Tensiometry determination

The surface tensions for the ternary mixture are measured at 298.15 K and 101.3 kPa using a maximum differential bubble pressure tensiometer (SensaDyne tensiometer model PC500-LV, USA). For experimental determination, the radii of the cylindrical glass probes were $r_1 = 0.125 \pm 0.01$ mm and $r_2 = 2.0 \pm 0.01$ mm, and the determination is carried out with a precision of ± 0.05 mN m⁻¹. Furthermore, the sample temperature is measured with a Pt 100 Ω probe and maintained under its isothermal conditions within ± 0.01 K using a Julabo thermostatic bath. The calibration procedures and experimental protocol have been broadly described and used to measure mixtures that involve cyclopentyl methyl ether or *n*-hexane or propan-1-ol, as we described in our previous studies.^{28,30-34,43}

3 Theoretical section

3.1 Vapor-liquid equilibria: data modeling and thermodynamical consistency

The experimental determination of the vapor-liquid phase equilibria (VLE) for the hexane + cyclopentyl methyl ether + propan-1-ol ternary mixture under the isobaric condition of $P = 94$ kPa considers the measurements of the equilibrium temperature T and the mole fractions of hexane (1), cyclopentyl methyl ether (2), and propan-1-ol (3) in both liquid (x_1, x_2, x_3) and vapor (y_1, y_2, y_3) phases. The experimental information is used to calculate the corresponding activity coefficients ($\gamma_1, \gamma_2, \gamma_3$), which are essential to quantify deviations from the ideal behavior of Raoult's law, to determine the excess molar Gibbs energy of the mixture ($G^E = RT \sum_{i=1}^3 x_i \ln \gamma_i$), and to assess the reliability of the experimental data (*i.e.*, thermodynamic consistency).

Considering that the VLE is measured at low pressure, the fugacity of the liquid phase is pressure-independent, and the vapor phase can be described as a perfect gas, the values of γ_i are calculated from the modified Raoult's law:⁴⁴

$$\gamma_i = \frac{y_i P}{x_i P_i^0} \quad (1)$$

where P_i^0 indicates the vapor pressure of component i , and the other terms have been previously defined. In the latter expression, the virial contribution was omitted because of the lack of experimental data regarding the cross-second virial coefficients or appropriate correlations, especially for the CPME binary subsystems.

In this work, experimental VLE data are validated by applying two thermodynamic consistency tests, namely the Wisniak LW method⁴⁵ and the Wisniak and Tamir method.⁴⁶ In the first test, thermodynamic consistency is assessed point by point using the following equation:

$$\frac{L_k}{W_k} = \frac{\left(\frac{\sum_{i=1}^3 x_i \Delta h_i^0}{\sum_{i=1}^3 x_i \Delta h_i^0 / T_i^0} - T \right)}{\left(\frac{RT}{\sum_{i=1}^3 x_i \Delta h_i^0 / T_i^0} \right) \left(\sum_{i=1}^3 x_i \ln \gamma_i - \sum_{i=1}^3 x_i \ln \left(\frac{y_i}{x_i} \right) \right)} \quad (2)$$

In the last equation, T_i^0 is the boiling temperature, and Δh_i^0 represents the enthalpy of vaporization of the pure fluid i evaluated at T_i^0 , R symbolizes the universal gas constant, T , x_i , and y_i represent the equilibrium conditions of temperature, and mole fractions for component i in the liquid and the vapor phases, respectively. γ_i is the activity coefficient for component i . This consistency test is proposed for equilibrium data at low pressure, and a point is declared consistent if it falls within the interval $0.90 < (L_k/W_k) < 1.10$.

The second consistency test considers the vapor pressure of pure fluids and the experimental uncertainties. This test evaluates the local deviation (D) (see eqn (3a)), and the local maximum deviation (D_{\max}) (see eqn (3b)) of two consecutive experimental points a and b , and declares consistency when $D < D_{\max}$.

$$D = \sum_{i=1}^3 (x_{ia} - x_{ib})(\ln \gamma_{ia} - \ln \gamma_{ib}) \quad (3a)$$

$$D_{\max} = \sum_{i=1}^3 (x_{ia} + x_{ib}) \left(\frac{1}{x_{ia}} + \frac{1}{y_{ia}} + \frac{1}{x_{ib}} + \frac{1}{y_{ib}} \right) \Delta x + \sum_{i=1}^3 (x_{ia} + x_{ib}) \frac{\Delta P}{P} + 2 \sum_{i=1}^3 |\ln \gamma_{ib} - \ln \gamma_{ia}| \Delta x + \sum_{i=1}^3 (x_{ia} + x_{ib}) B_j \left[(T_a + C_j)^{-2} + (T_b + C_j)^{-2} \right] \Delta T \quad (3b)$$

In this equation ΔT , ΔP , and Δx represent the experimental uncertainties in the measurements of temperature (T), pressure (P), and mole fraction (x_i), respectively. Based on the VLE and GC devices, these uncertainties are $\Delta T = \pm 0.1$ K, $\Delta P = \pm 0.1$ kPa, and $\Delta x_i = \pm 0.001$. In eqn (3b), B_j and C_j represent the coefficients of the Antoine vapor pressure expression for pure fluids, which is given by the expression:

$$\log(P_i^0 / \text{kPa}) = A_i - \frac{B_i}{(T/K) + C_i} \quad (4)$$

The corresponding numerical values for T_i^0 , Δh_i^0 , A_i , B_i , and C_i for CPME, *n*-hexane, and propan-1-ol will be described in the Results and discussion section.

3.2 Molecular-based equation of state: SAFT-VR Mie EoS

Theoretical thermodynamic modeling of the ternary mixture is based on the molecular-based SAFT-VR Mie equation of state



(EoS),⁴¹ which predicts the VLE and the liquid mass density and is the fundamental basis for the prediction of the other thermophysical properties measured in this work (*i.e.*, liquid viscosity, and surface tension).

In general terms, the Helmholtz energy, A , for a pure fluid or a fluid mixture in the SAFT-VR Mie EoS is given by the sum of the different contributions to the Helmholtz energy. For the case of the ternary mixture explored in this work, A is formed from the ideal gas contribution, A^{IG} , the monomer segments, A^{MONO} , molecular chain formation, A^{CHAIN} , and the intermolecular association, A^{ASSOC} . The reader is redirected to the original studies^{41,47} for a complete description of each Helmholtz energy term and their extension for mixtures. From the original reports, it is possible to observe that non-associate fluids are characterized by five parameters, namely the effective segment diameter, σ , the segment number, m_s , the dispersion energy, ε , and the repulsive, λ_r , and attractive λ_a Mie potential exponents. Furthermore, for associate fluids, two additional parameters are needed: the interaction site-site energy, ε^{AB} , and the range of association, r_c^{AB} , and it is also necessary to define the association scheme. The association scheme can be described using the original Huang and Radosz scheme⁴⁸ or in a compact form by using three numbers: number of bipolar sites, B , number of positive sites, P , and number of negative sites, N .⁴⁹ The corresponding numerical values for the parameters of pure fluids in the SAFT-VR Mie EoS will be described in the Results and discussion section.

For the case of mixtures, the SAFT-VR Mie only considers binary interactions, where the unlike binary parameters for Mie exponents, λ_{ij} , size, σ_{ij} , and dispersion energy, ε_{ij} , are given by the following expressions:

$$(\lambda_{ij} - 3) = \sqrt{(\lambda_{ii} - 3)(\lambda_{jj} - 3)} \quad (5)$$

$$\sigma_{ij} = \frac{(\sigma_{ii} + \sigma_{jj})}{2} \quad (6)$$

$$\varepsilon_{ij} = \frac{\sqrt{\sigma_{ii}^3 \sigma_{jj}^3}}{\sigma_{ij}^3} (1 - k_{ij}) \quad (7)$$

where k_{ij} is a binary interaction parameter obtained by fitting experimental phase equilibrium data for binary systems. Additionally, the interaction between non-associate fluid and associate fluid is characterized by a parameter r_c^{AB} , which provides an approximate route to evaluate the interaction site-site energy parameter, ε^{AB} . In this work, r_c^{AB} will be fitted for the binary interactions between propan-1-ol with CPME and propan-1-ol with *n*-hexane. The corresponding numerical values were obtained from previous studies and will be described in the Results and discussion section.

3.3 Determination of the vapor-liquid equilibria and the liquid mass density from SAFT-VR Mie EoS

The isobaric vapor-liquid equilibria (VLE) for a ternary mixture can be predicted using the following expressions:^{44,50}

$$T^{\text{L}} = T^{\text{V}} = T \quad (8)$$

$$f_i = \mu_i(T^{\text{L}}, V^{\text{L}}, \underline{x}) - \mu_i(T^{\text{V}}, V^{\text{V}}, \underline{y}); i = 1, 2, 3 \quad (9)$$

$$f_4 = A_{\text{V}}(T^{\text{L}}, V^{\text{L}}, \underline{x}) - A_{\text{V}}(T^{\text{V}}, V^{\text{V}}, \underline{y}) = 0 \quad (10)$$

$$f_5 = P^0 + A_{\text{V}}(T, V^{\text{V}}, V^{\text{L}}) \quad (11)$$

Eqn (8)–(10) are the classical phase equilibrium conditions, namely the temperature is equal in both phases (eqn (8)), the chemical potentials of each of the components in each of the phases are equal (eqn (9)) and the pressure is equal in both phases (eqn (10) and eqn (11)) reflects the restriction for isobaric conditions, here $P^0 = 94.00$ kPa. In the latter expressions, the superscripts L and V denote the liquid and vapor bulk phases, respectively. T denotes the temperature, μ_i symbolizes the chemical potential of the component i , which is calculated from the Helmholtz energy, A , according to $\mu_i = (\partial A / \partial n_i)_{T, V, n_j \neq i}$ and $A_{\text{V}} = (\partial A / \partial V)T, n$.

Substituting eqn (8) into eqn (9)–(11) and considering that the mole fractions are restricted by $\sum_{i=1}^3 x_i = 1$ and $\sum_{i=1}^3 y_i = 1$, eqn (9)–(11) are solved under the conditions: $f_1 = f_2 = f_3 = f_4 = f_5 = 0$, in other words, given $[P, \underline{x}]$, the bubble T provides $[T, \underline{y}, V^{\text{V}}, V^{\text{L}}]$. A detailed explanation of this calculation method can be found in our previous work.⁵¹

The liquid mass density of the mixture at $T = 298.15$ K and $P = 101.3$ kPa is calculated as a function of the liquid mole fraction, \underline{x} , using the expression:

$$f_6 = P + A_{\text{V}}(V^{\text{L}}, \underline{x}) \quad (12)$$

where the liquid mass density is predicted by solving $f_6 = 0$ and $\rho = 1/V^{\text{L}}$.

3.4 Thermodynamical modeling of liquid viscosity

The liquid viscosity for the ternary mixture, η , is predicted using Helmholtz scaling theory (A-scaling), where the residual Helmholtz energy is described through the SAFT-VR Mie EoS. The theoretical framework of this theory is based on an *ansatz* function of the difference between the molar Helmholtz energy of the system, \bar{A} , and that of the reference system, in this case, the hard-sphere contribution, \bar{A}_{HS} . Mathematically, η is given by the following expression:⁴²

$$\ln\left(\frac{\eta}{\eta^{\text{HS}}}\right) = f\left(\Psi \left[\left(\frac{\bar{A}}{RT} \right) - \left(\frac{\bar{A}_{\text{HS}}}{RT} \right) \right] \right) = f\left(\frac{\Psi \bar{A}^*}{RT}\right) \quad (13)$$

where \bar{A} is calculated using the SAFT-VR Mie EoS, as previously described. The theoretical model implies calculating the Helmholtz energy of the system without the hard-sphere contribution. This contribution is present in the monomer contribution (A^{MONO}). Ψ is an empirical factor, which is defined as a reduced temperature function ($T^* = (k_B T / \varepsilon)$) with a substance-dependent parameter, θ , that is $\Psi = (T^*)^\theta$.

In eqn (13), η^{HS} is the viscosity of a hard-sphere, which can be calculated from the Chapman-Enskog equation:⁵²

$$\eta^{\text{HS}} = \frac{5}{16} \frac{\sqrt{\frac{M_i T^* \varepsilon}{N_{\text{av}} \pi}}}{\sigma^2 Q^{(2,2)*}} \quad (14)$$



where M_i is the molecular weight of the component i , T^* symbolizes the reduced temperature, ε is the dispersion energy, N_{av} is the Avogadro constant, and σ is the effective segment diameter. The collision integral, $\Omega^{(2,2)*}$, is calculated using the empirical expression proposed by Neufeld:⁵³

$$\begin{aligned} \Omega^{(2,2)*} = & \frac{1.16145}{T^{*0.14874}} + \frac{0.52487}{\exp(0.7732T^*)} \\ & + \frac{2.16178}{\exp(2.43787T^*)} - 6.435 \times 10^{-4} T^{*0.14874} \\ & \times \sin(18.0323T^{*-0.7683} - 7.27371) \end{aligned} \quad (15)$$

For the case of pure fluids, the Helmholtz scaling model uses the *ansatz* function Ψ as a third-degree polynomial:

$$\ln\left(\frac{\eta}{\eta^{\text{HS}}}\right) = a + b\left(\frac{\Psi \bar{A}^*}{RT}\right) + c\left(\frac{\Psi \bar{A}^*}{RT}\right)^2 + d\left(\frac{\Psi \bar{A}^*}{RT}\right)^3 \quad (16)$$

where a , b , c , and d are substance-dependent parameters and are adjusted from experimental data on the viscosity of pure fluids. The corresponding numerical values will be described in the Results and discussion section.

For the case of mixtures of n_c components, the *ansatz* for mixtures is described by the following expression:⁴²

$$\begin{aligned} \ln\left(\frac{\eta_{\text{mix}}}{\eta^{\text{HS}}}\right) = & \sum_{i=1}^{n_c} x_i a_i + \sum_{i=1}^{n_c} x_i b_i \left(\Psi_i \frac{m_{si}}{\bar{m}_s} \frac{\bar{A}^*}{RT}\right) \\ & + \sum_{i=1}^{n_c} x_i c_i \left(\Psi_i \frac{m_{si}}{\bar{m}_s} \frac{\bar{A}^*}{RT}\right)^2 \\ & + \sum_{i=1}^{n_c} x_i d_i \left(\Psi_i \frac{m_{si}}{\bar{m}_s} \frac{\bar{A}^*}{RT}\right)^3 \end{aligned} \quad (17)$$

where a_i , b_i , c_i and d_i are the same substance-dependence parameters calculated for pure fluids. \bar{m} is the mean number of segments, which is calculated from the following equation:

$$\bar{m}_s = \sum_{i=1}^{n_c} x_i m_{si} \quad (18)$$

The Chapman–Enskog viscosity for mixtures is obtained from Wilke's approximation:⁵⁴

$$\eta_{\text{mix}}^{\text{HS}} = \sum_{i=1}^c \frac{\eta_i^{\text{HS}}}{1 + \frac{1}{x_i} \sum_{j=1}^c x_j \phi_{ij}} \quad (19)$$

where ϕ_{ij} is given by the equation:

$$\phi_{ij} = \frac{\left[1 + \sqrt{\eta_i^{\text{HS}}/\eta_j^{\text{HS}}} (M_j/M_i)\right]^2}{\sqrt{8(1 + M_i/M_j)}} \quad (20)$$

where M_i is the molecular weight of the component i .

From eqn (13)–(20), it is possible to observe that the determination of the viscosity of the mixtures depends only on the

parameters of the pure components. Therefore, this theory provides a route to fully predict the viscosity of mixtures.

3.5 Thermodynamical modeling of interfacial properties of the mixtures

The concentration profiles, ρ_i , along the interfacial region, z , $\rho_i(z)$ and the surface tension, σ , of the mixtures are predicted from the van der Waals Square Gradient Theory (SGT)^{37–39} using the SAFT-VR Mie model for the homogeneous Helmholtz energy contribution.

In the SGT, the $\rho_i(z)$ profiles are obtained by solving the following system of differential equations:

$$\sum_{j=1}^{n_c} (1 - \beta_{ij}) \sqrt{c_{ij} c_{jj}} \frac{d^2 \rho_j}{dz^2} = \mu_i - \mu_i^0; \quad i = 1, 2, \dots, n_c \quad (21)$$

Eqn (21) is restricted to the boundary conditions given by the bulk density of each phase, namely $\rho_i|_{z=-\infty} = \rho_i^V$ and $\rho_i|_{z=+\infty} = \rho_i^L$. In the above equations, μ_i represents the chemical potential of component i , which is given by the SAFT-VR Mie EoS model considering that $\rho_i(z)$, μ_i^0 is the chemical potential of component i evaluated at phase equilibrium, c_{ii} symbolizes the influence parameter of the pure fluid i , and β_{ij} is an adjustable binary parameter of SGT.

Solving eqn (21) yields the concentration profiles for species that connect the two bulk phases in a planar interface, which are used to calculate the surface tension of the mixture using the expression:^{37–39}

Table 3 Experimental measurements of vapor–liquid phase equilibria (VLE) for *n*-hexane (1) + CPME (2) + propan-1-ol (3) ternary mixture at 94.00 kPa^a

T/K	x_1	x_2	y_1	y_2	T/K	x_1	x_2	y_1	y_2
365.21	0.076	0.818	0.227	0.571	345.45	0.244	0.225	0.611	0.103
362.83	0.071	0.733	0.218	0.487	341.80	0.253	0.122	0.673	0.052
361.01	0.073	0.635	0.231	0.411	340.77	0.349	0.120	0.713	0.043
359.68	0.068	0.545	0.250	0.354	343.01	0.351	0.210	0.679	0.079
358.49	0.072	0.440	0.277	0.295	345.12	0.361	0.303	0.647	0.118
357.27	0.071	0.343	0.315	0.238	347.56	0.356	0.411	0.615	0.169
356.16	0.059	0.239	0.324	0.184	349.69	0.371	0.493	0.614	0.219
352.13	0.069	0.130	0.417	0.104	346.53	0.465	0.405	0.685	0.158
348.17	0.135	0.125	0.541	0.080	344.06	0.463	0.308	0.689	0.112
349.87	0.137	0.222	0.498	0.135	341.99	0.459	0.208	0.710	0.073
352.68	0.131	0.325	0.454	0.182	339.55	0.459	0.115	0.746	0.035
354.37	0.129	0.421	0.404	0.239	339.05	0.560	0.110	0.764	0.032
355.55	0.139	0.516	0.387	0.284	341.25	0.528	0.213	0.732	0.069
356.71	0.149	0.603	0.382	0.333	343.32	0.551	0.298	0.732	0.101
358.68	0.161	0.695	0.382	0.408	340.95	0.649	0.213	0.773	0.068
354.30	0.246	0.610	0.507	0.303	338.51	0.667	0.118	0.788	0.031
351.91	0.246	0.512	0.506	0.247	339.00	0.750	0.135	0.813	0.037
349.86	0.250	0.416	0.536	0.194	340.71	0.754	0.184	0.831	0.058
348.17	0.241	0.325	0.568	0.149	338.08	0.814	0.084	0.837	0.015

^a Standard uncertainties, u , are: $u(P) = 0.03$ kPa, $u(T) = 0.01$ K, and $u(x_i) = u(y_i) = 0.001$, where T denotes the equilibrium temperature and x_i and y_i are mole fractions in liquid and vapor phases, respectively, of component i .



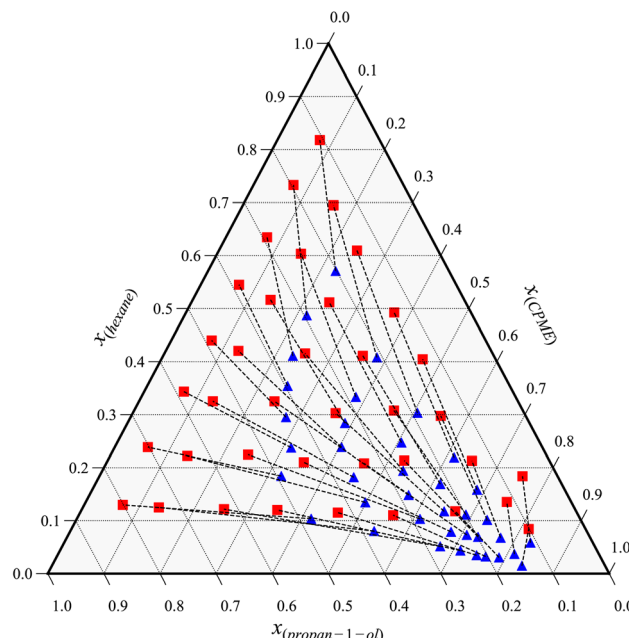


Fig. 1 Experimental data of the vapor–liquid phase equilibria (VLE) for the *n*-hexane (1) + CPME (2) + propan-1-ol (3) ternary mixture at 94.00 kPa. (■) liquid phase; (▲) vapor phase; (—) tie lines.

$$\sigma = \sum_{i,j=1}^{n_c} \int_{-\infty}^{+\infty} (1 - \beta_{ij}) \sqrt{c_{ii} c_{jj}} \frac{d\rho_i}{dz} \frac{d\rho_j}{dz} dz \quad (22)$$

Based on eqn (21) and (22), the SGT needs the c_{ii} and β_{ij} , which are adjusted using experimental surface tension data of pure fluids and binary mixtures, respectively. The numerical values of c_{ii} and β_{ij} will be discussed in the Results and discussion section. Considering the need for information on SGT, it is possible to remark that this theory for ternary mixtures is fully predictive. In this work, the SGT is solved by using the methodology described in our previous work.⁵¹

4 Results and discussion

In this section, the thermophysical properties (*i.e.*, phase equilibria, liquid mass densities, liquid viscosity, and surface tensions) for the *n*-hexane (1) + CPME (2) + propan-1-ol (3) ternary mixture are experimentally and theoretically reported.

4.1 Vapor–liquid equilibria for the *n*-hexane (1) + CPME (2) + propan-1-ol (3) ternary mixture at 94.00 kPa

The experimental determination of the vapor–liquid equilibrium (VLE) data for the *n*-hexane (1) + CPME (2) + propan-1-ol (3) ternary mixture at 94.00 kPa is summarized in Table 3.

Complementary to the previous experimental data for the ternary mixture, Fig. 1 displays the VLE determination together with the liquid–vapor tie lines.

From Fig. 1, it is possible to observe that this mixture does not exhibit ternary azeotropy behavior within the measurement range. This conclusion is also verified by evaluating the relative volatility function, FO^{Az} , which was proposed by Gmehling *et al.*⁵⁵

$$FO^{Az} = |\alpha_{12} - 1| + |\alpha_{13} - 1| + |\alpha_{23} - 1| \quad (23)$$

where α_{ij} denotes the relative volatility of the component *i* with respect to the component *j* ($\alpha_{ij} = (y_j/x_i)/(y_i/x_j)$). Based on the function of Gmehling *et al.*⁵⁵ $FO^{Az} = 0$ at the azeotropic point. For the case of the ternary mixture explored here $FO^{Az} > 0$ in the entire mole fraction range, indicating zeotropic behavior.

For the purpose of calculating the experimental values of γ_i , which are needed to quantify deviation type, G^E and to evaluate thermodynamic consistency, Table 4 summarizes the thermophysical properties of the pure fluids involved in reported determinations, which were obtained in previous studies by using the same devices used here.^{30,31,34} Based on the experimental data and using eqn (1), the activity coefficients are always positive, $\gamma_i > 1$ denoting a positive deviation from Raoult's law, and $G^E > 0$ in the whole mole fraction range.

Table 4 Antoine's constants (see eqn (4)), boiling points T_i^0 and enthalpy of vaporization, Δh_i^0 , for pure fluids^a

Fluid	A_i	B_i	C_i	Temperature range/K	T_i^0 (K)	Δh_i^0 (kJ mol ⁻¹)
CPME ^b	6.5772	1636.3534	-20.3705	341.31 to 378.40	378.32	33.00
<i>n</i> -Hexane ^c	6.25283	1310.6332	-33.2066	307.67 to 342.08	341.94	28.95
Propan-1-ol ^d	7.00710	1517.6000	-66.8030	341.26 to 370.24	370.25	41.66

^a The Antoine constants and the boiling points were obtained from: ^b Mejía and Cartes.³¹ ^c Mejía *et al.*³⁰ ^d Mejía *et al.*,³⁴ enthalpies of vaporization were obtained from the NIST database.⁵⁶

Table 5 Pure fluid molecular parameters for SAFT-VR Mie EoS^a

Fluid	m_s	$\sigma/\text{\AA}$	$\varepsilon/k_B/\text{K}$	λ_r	$\varepsilon^{AB}/k_B/\text{K}$	r_c^{AB}/σ	$[B,P,N]$
CPME ^b	2.3418	4.1254	344.81	14.177	—	—	[0,0,1]
<i>n</i> -Hexane ^b	1.9672	4.5476	377.60	18.411	—	—	[0,0,0]
Propan-1-ol ^c	2.2513	3.6008	253.45	11.960	2794.88	0.3481	[1,0,1]

^a The molecular parameters were taken from. ^b Mejía *et al.*³⁰ ^c Cripwell *et al.*,⁵⁷ $\lambda_a = 6$ for all fluids.



Table 6 SAFT-VR Mie binary interaction parameters for *n*-hexane (1) + CPME (2), *n*-hexane (1) + propan-1-ol (3), CPME (2) + propan-1-ol (3) mixtures and their deviations

Mixtures	k_{ij}	$r_{c,ij}^{\text{AB}}/\text{\AA}$	% ΔP^a	% Δy^b
(1) + (2) ^c	0.00295	—	1.17	0.37
(1) + (3) ^d	0.00423	1.312	3.82	1.96
(2) + (3) ^e	0.01230	2.206	0.81	0.53

^a % $\Delta P = (100/N_d) \sum_{i=1}^{N_d} |P_i^{\text{exp}} - P_i^{\text{cal}}|/P_i^{\text{exp}}$.

^b % $\Delta y = (100/N_d) \sum_{i=1}^{N_d} |y_i^{\text{exp}} - y_i^{\text{cal}}|$. The experimental data of VLE were taken from. ^c Mejía *et al.*³⁰ ^d Prabhu and van Winkle.⁵⁸ ^e Mejía *et al.*³⁴

In order to validate the reliability of the VLE data reported here, the thermodynamic consistency was evaluated using both tests. In the first case, the Wisniak LW test shows that the values fall within the range $0.93 < L_k/W_k < 0.95$, and the second test reports that all the values of D were found to be less than D_{max} ,

with the latter being equal to 0.0417. Therefore, it is possible to state that the measured VLE equilibrium data are considered thermodynamically consistent.

With the aim of predicting the VLE experimental data reported in Table 3, the SAFT-VR Mie EoS requires pure and binary parameters. For the case of pure fluid parameters (*i.e.*, m_s , σ , ε , λ_r , λ_a , r_c^{AB} , and $[B, P, N]$) these values are already available and are summarized in Table 5.

On the other hand, the SAFT-VR Mie EoS binary parameters (k_{ij} , and $r_{c,ij}^{\text{AB}}$) are obtained using the experimental measurements of the sub-binaries that conform to the ternary mixture. Specifically, the experimental data for *n*-hexane (1) + CPME (2) and CPME (2) + propan-1-ol (3) binary mixtures were taken from our previous experimental studies at 94 kPa,^{30,34} while the experimental data for *n*-hexane (1) + propan-1-ol (3) binary mixture were taken from Prabhu and van Winkle⁵⁸ who reported VLE at 101.30 kPa. Table 6 summarizes the corresponding numerical values and their deviations.

The performance of the SAFT-VR Mie EoS in predicting this ternary mixture can be evaluated by comparing the prediction to the experimental data, as illustrated in Fig. 2, which displays the corresponding parity plots for temperature (Fig. 2a) and vapor mole fractions (Fig. 2b), where it is possible to observe that the predictions can be considered acceptable when compared to experimental data. Additionally, Table 7 collects the corresponding statistical deviations obtained by computing the dew and bubble points, which confirm the capability of the SAFT-VR Mie to predict the VLE.

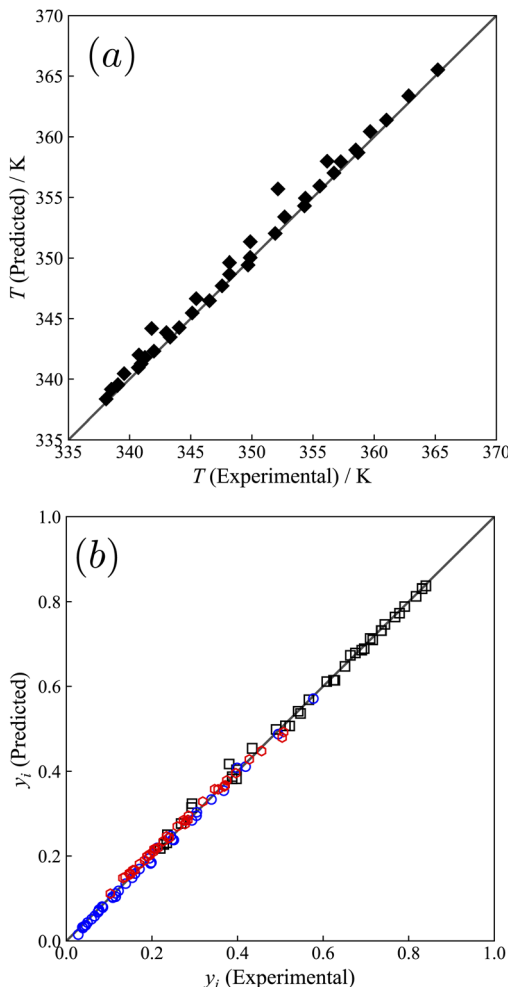


Fig. 2 Vapor–liquid equilibria parity plot for the *n*-hexane (1) + CPME (2) + propan-1-ol (3) ternary mixture at 94.00 kPa. (a) Equilibria temperature. (b) Vapor mole fractions: ○: CPME; □: *n*-hexane; ◇: propan-1-ol.

Table 7 Statistical deviation in bubble and dew point calculations for the *n*-hexane (1) + CPME (2) + propan-1-ol (3) ternary mixture^a

Pressure bubble point			
% ΔP	% Δy_1	% Δy_2	% Δy_3
2.06	0.71	1.33	1.01
Pressure dew point			
% ΔP	% Δx_1	% Δx_2	% Δx_3
1.93	1.09	2.42	3.16
Temperature bubble point			
% ΔT	% Δy_1	% Δy_2	% Δy_3
0.18	0.81	1.33	0.98
Temperature dew point			
% ΔT	% Δx_1	% Δx_2	% Δx_3
0.15	0.92	2.37	2.94

^a % $\Delta \vartheta = (100/N_d) \sum_{i=1}^{N_d} |\vartheta_i^{\text{exp}} - \vartheta_i^{\text{cal}}|/\vartheta_i^{\text{exp}}$ with $\vartheta = P$ or T .

% $\Delta \theta = (100/N_d) \sum_{i=1}^{N_d} |\theta_i^{\text{exp}} - \theta_i^{\text{cal}}|$ with $\theta = x_i$ or y_i .



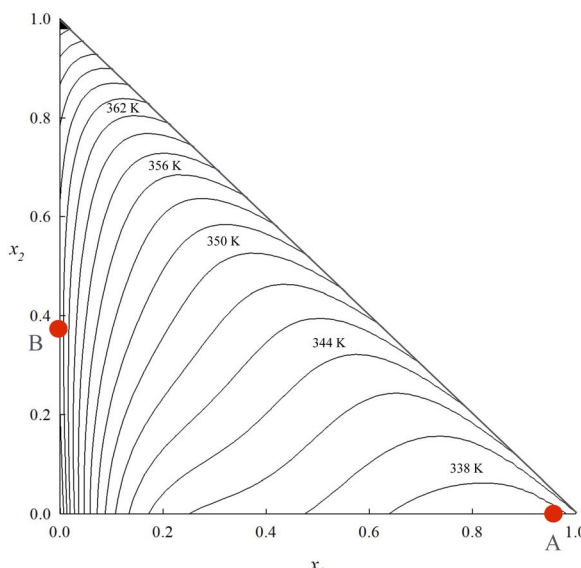


Fig. 3 Bubble temperature diagram of the ternary system *n*-hexane (1) + CPME (2) + propan-1-ol (3) at 94.00 kPa. The vapor–liquid equilibrium data were obtained using the SAFT-VR Mie equation of state. (A, B) Binary azeotropes for the binary systems composed of *n*-hexane (1) + propan-1-ol (3) ($x_1^{\text{Aze}} = 0.9436$, and $T^{\text{Aze}} = 338.85$ K) and CPME (2) + propan-1-ol (3) ($x_3^{\text{Aze}} = 0.3980$, and $T^{\text{Aze}} = 365.15$ K), respectively.

Finally, Fig. 3 shows the theoretical VLE predictions in the T – x_1 – x_2 phase diagram (map of isotherms) for the ternary system at 94.00 kPa. From this diagram, it is possible to conclude that, although the binaries that contain propan-1-ol exhibit positive azeotropy (see points A, B in Fig. 3), no ternary azeotrope is present in the ternary mixture.

Considering the high capability of the SAFT-VR Mie EoS to describe the VLE, this model can be applied to other isobaric conditions to explore the impact of the pressure on the VLE behavior. Based on Elvers and Schütze textbook,⁷ an appropriate pressure range for industrial plant applications covers the range from 70 kPa to 120 kPa. Fig. 4 condenses the VLE under three isobaric conditions within this range, where it is

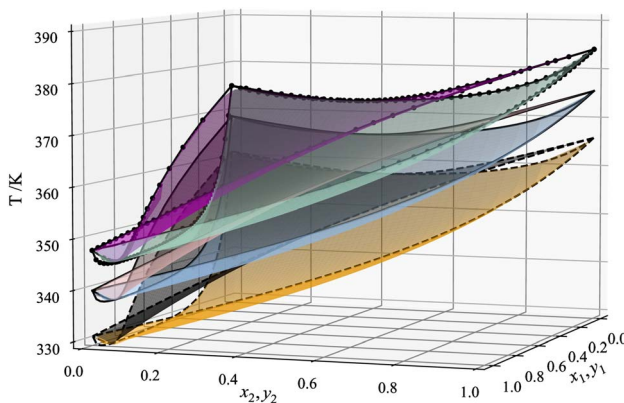


Fig. 4 Vapor–liquid equilibrium for the hexane (1) + cyclopentyl methyl ether (2) + propan-1-ol (3) ternary mixture under three isobaric conditions: (down) 70 kPa; (middle) 94 kPa, (high) 120 kPa.

Table 8 Experimental liquid mass densities for the *n*-hexane (1) + CPME (2) + propan-1-ol (3) ternary liquid mixture at 298.15 K and 101.30 kPa^a

x_1	x_2	$\rho/\text{kg m}^{-3}$	x_1	x_2	$\rho/\text{kg m}^{-3}$
0.090	0.102	787.71	0.368	0.106	736.65
0.084	0.206	798.16	0.362	0.209	747.84
0.088	0.297	805.36	0.395	0.327	753.45
0.082	0.402	813.79	0.374	0.422	764.17
0.089	0.522	819.41	0.371	0.524	771.48
0.093	0.621	824.74	0.481	0.101	719.82
0.082	0.714	830.96	0.374	0.215	746.69
0.085	0.811	833.90	0.376	0.319	754.59
0.176	0.099	770.82	0.374	0.422	762.77
0.170	0.207	781.47	0.373	0.524	771.04
0.175	0.308	788.85	0.477	0.103	720.24
0.174	0.419	796.17	0.483	0.213	730.24
0.173	0.534	803.71	0.472	0.318	741.64
0.181	0.616	808.08	0.475	0.419	748.50
0.171	0.726	815.08	0.575	0.110	709.62
0.265	0.103	754.03	0.577	0.209	716.19
0.266	0.205	763.92	0.569	0.323	730.45
0.256	0.312	773.79	0.671	0.113	696.91
0.266	0.434	782.05	0.669	0.223	707.72
0.264	0.530	788.46	0.785	0.103	685.65
0.262	0.634	795.11			

^a x_i represents the mole fractions of component i , ρ is the liquid mass density. The standard uncertainties, u , are: $u(P) = 1$ kPa, $u(T) = 0.01$ K, and $u(x_i) = 0.001$. The combined expanded uncertainty, U_c , with a 95% confidence level ($k = 2$): $U_c(\rho) = 0.1$ kg m⁻³.

possible to observe the evolution of the phase equilibria and their binary azeotropic behaviour. All the reported results (*i.e.*, statistical deviation in bubble and dew point, the parity plots for temperature and vapor mole fractions, and the ternary VLE diagram can be reproduced using the “Vapor Liquid Equilibria.ipynb” Jupyter notebook, which is available as an open-source on our GitHub repository.⁵⁹

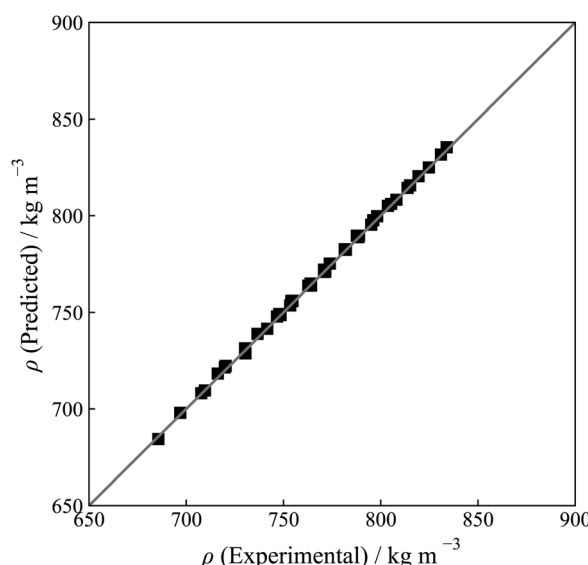


Fig. 5 Liquid mass density parity plot for the *n*-hexane (1) + CPME (2) + propan-1-ol (3) ternary mixture at 298.15 K and 101.30 kPa.



4.2 Liquid mass densities for the hexane (1) + CPME (2) + propan-1-ol (3) ternary mixture at 298.15 K and 101.3 kPa

The experimental liquid mass densities (ρ) as a function of the liquid mole fractions (x_1, x_2) at 298.15 K and 101.3 kPa for the ternary system are presented in Table 8 together with the associated standard deviations.

The theoretical predictions of the liquid mass densities for the system were calculated using the SAFT-VR Mie EoS, as described by eqn (12). The results indicate that this model has a high capability to predict the ternary system's behavior, achieving an average absolute deviation of 0.128%, as can be observed in the parity plot displayed in Fig. 5.

Complementarily, Fig. 6 shows a contour plot of the liquid mass densities for the ternary system across the full composition range obtained using the molecular-based model at the isobaric condition of 101.3 kPa and under two isothermal conditions, namely 298.15 K and 313.15 K, the latter corresponds to the optimal temperature for evaluating optimal

engine performance.⁷ From these figures, it is possible to conclude that the liquid mass density displays similar behavior under the two isothermal conditions.

The “Vapor Liquid Equilibria.ipynb” Jupyter notebook includes a subroutine to compute the liquid mass density of the mixture and can be used to generate the parity density and contour density plots. The open-source code is available from our GitHub repository.⁵⁹

4.3 Liquid viscosities for the *n*-hexane (1) + CPME (2) + propan-1-ol (3) ternary mixture at 298.15 K and 101.30 kPa

Table 9 collects the experimental liquid viscosity data (η) as a function of the liquid mole fractions (x_1, x_2) at 298.15 K and 101.3 kPa for the ternary system together with the associated standard deviations.

As was stated in the theoretical Section, the liquid viscosities for the ternary system can be fully predicted from the Helmholtz-scaling theory (A-scaling) combined with the SAFT-VR Mie EoS only using pure fluid parameters. For the case of SAFT-VR Mie EoS, the corresponding molecular parameters are already summarized in Table 5, while A-scaling uses the descriptive variables (θ, a_i, b_i, c_i , and d_i) for each pure fluid. These values are fitted using experimental data from previous studies and the available literature.^{29,56} The corresponding numerical values are summarized in Table 10.

Using the parameters reported in Table 10, the viscosity of the pure fluids can be described with an average absolute deviation less than 0.06% in a wide temperature range at 101.3 kPa, and also the viscosity of sub-binary systems is predicted

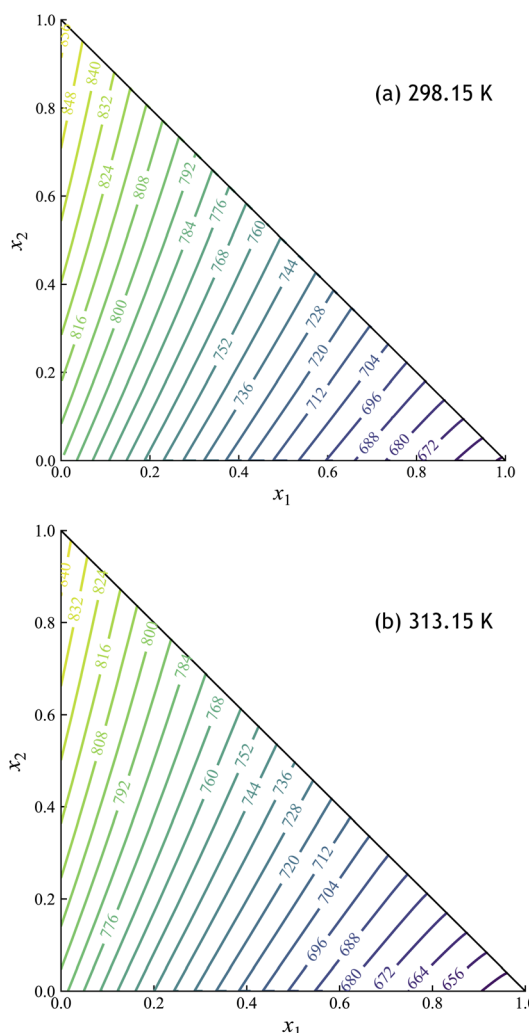


Fig. 6 Contour plot of the liquid mass densities (ρ in kg m^{-3}) for the mixture of *n*-hexane (1) + CPME (2) + propan-1-ol (3) under two isothermal conditions ((a): 298.15 K and (b): 313.15 K) and isobaric (101.30 kPa) conditions obtained using SAFT-VR Mie EoS.

Table 9 Experimental liquid viscosities (η) for the *n*-hexane (1) + CPME (2) + propan-1-ol (3) ternary liquid mixture at 298.15 K and 101.30 kPa^a

x_1	x_2	$\mu/\text{mPa s}$	x_1	x_2	$\mu/\text{mPa s}$
0.090	0.102	1.1540	0.368	0.106	0.5930
0.084	0.206	0.9530	0.362	0.209	0.5190
0.088	0.297	0.8110	0.395	0.327	0.4370
0.082	0.402	0.7080	0.374	0.422	0.4180
0.089	0.522	0.6080	0.371	0.524	0.3950
0.093	0.621	0.5600	0.481	0.101	0.4830
0.082	0.714	0.5260	0.374	0.215	0.5070
0.085	0.811	0.4920	0.376	0.319	0.4520
0.176	0.099	0.9350	0.374	0.422	0.4180
0.170	0.207	0.7760	0.373	0.524	0.3940
0.175	0.308	0.6650	0.477	0.103	0.4840
0.174	0.419	0.5820	0.483	0.213	0.4250
0.173	0.534	0.5200	0.472	0.318	0.3990
0.181	0.616	0.4800	0.475	0.419	0.3750
0.171	0.726	0.4540	0.575	0.110	0.4130
0.265	0.103	0.7480	0.577	0.209	0.3760
0.266	0.205	0.6310	0.569	0.323	0.3550
0.256	0.312	0.5610	0.671	0.113	0.3610
0.266	0.434	0.4880	0.669	0.223	0.3390
0.264	0.530	0.4510	0.785	0.103	0.3250
0.262	0.634	0.4230			

^a x_i represents the mole fractions of component i , η is the liquid viscosity. The standard uncertainties, u , are: $u(P) = 1 \text{ kPa}$, $u(T) = 0.01 \text{ K}$, and $u(x_i) = 0.001$. The combined expanded uncertainty, U_c , with a 95% confidence level ($k = 2$): $U_c(\eta) = 0.02 \text{ mPa s}$.



Table 10 Helmholtz scaling parameters^a

Fluid	θ	a	b	c	d
CPME ^b	1.7735	1.4168	-2.0518	-0.5047	-0.0518
<i>n</i> -Hexane ^b	0.7019	3.6514	-0.3226	-0.0014	-0.0010
Propan-1-ol ^c	1.8740	0.5753	-1.4603	-0.1867	-0.0106

^a The values are fitted from experimental data. ^b Cartes *et al.*²⁹ ^c NIST database.⁵⁶

with low deviations in the whole mole fraction at 298.15 K and 101.3 kPa. Specifically, the model predicts the following absolute percentage deviations for the involved binary mixtures: 1.45% for *n*-hexane (1) + CPME (2),²⁹ 3.84% for *n*-hexane (1) + propan-1-ol (3),⁶⁰ and 2.53% for CPME (2) + propan-1-ol (3). The latter binary mixture has been measured and predicted here due to the lack of experimental and theoretical information. Both experimental data and modeling are summarized in the ESI.

For the ternary system, the molecular-based method performs an excellent prediction of the viscosity of the mixture in the whole mole fraction range, as can be seen in the parity plot shown in Fig. 7 with an absolute average deviation of 2.03%.

The high performance of the A-scaling can be attributed to the greater dependence on molecular parameters, as the accuracy of the prediction strongly relies on the performance of the EoS in calculating thermodynamic properties. Furthermore, A-scaling has the significant advantage of not requiring an extra parameter, neither binary mixtures nor multi-component systems, which is a plus when aiming to reproduce the behavior of transport properties such as viscosity in the whole mole fraction range, as observed in Fig. 8, which displays the contour plot for the viscosity calculated using A-scaling + SAFT-

VR Mie EoS under the isobaric condition of 101.3 kPa and under the same isothermal conditions used in the liquid mass density (*i.e.*, 298.15 and 313.15 K). As we stated before, the isothermal condition of 313.15 K corresponds to the optimal temperature for evaluating optimal engine performance.⁷

All results reported in this section, *i.e.*, parameter determination, the descriptive variables (θ , a_i , b_i , c_i , and d_i) of pure fluids and their liquid viscosity as a function of temperature and the liquid viscosity for the ternary mixture, *i.e.*, the parity and contour viscosity plots, can be reproduced using The Jupyter-Notebook “Liquid viscosities – Scaling theory.ipynb” which is available as an open-source on our GitHub repository.⁵⁹

4.4 Surface properties for the hexane (1) + CPME (2) + propan-1-ol (3) ternary mixture at 298.15 K and 101.30 kPa

The tensiometry determinations (*i.e.*, surface tensions), σ , as a function of the liquid mole fractions (x_1 , x_2) for this ternary

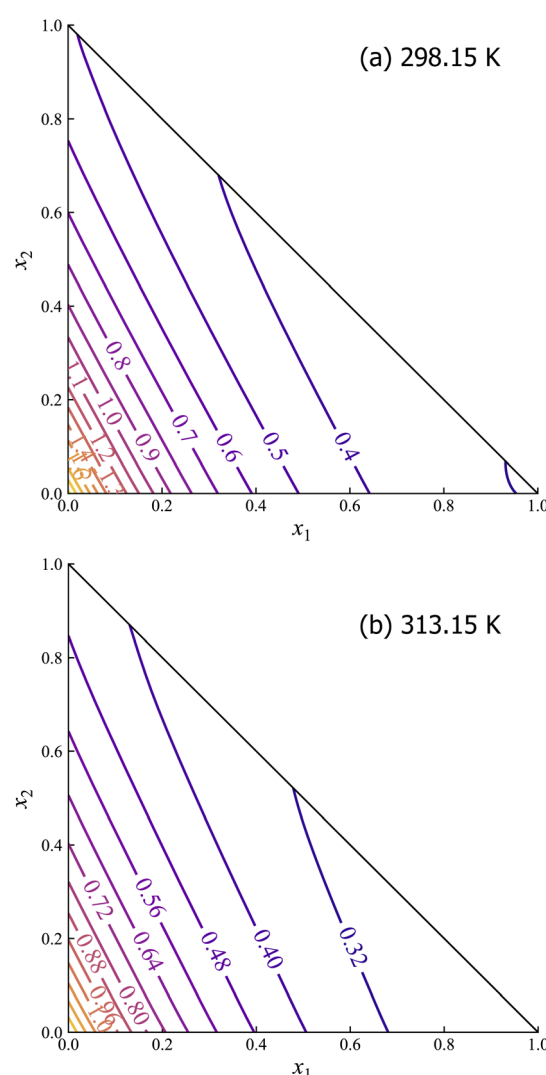


Fig. 8 Contour plot of the liquid viscosities (η in mPa s) for the mixture of *n*-hexane (1) + CPME (2) + propan-1-ol (3) under two isothermal conditions ((a): 298.15 K and (b): 313.15 K) and isobaric (101.30 kPa) conditions obtained using SAFT-VR Mie + A-scaling theory.

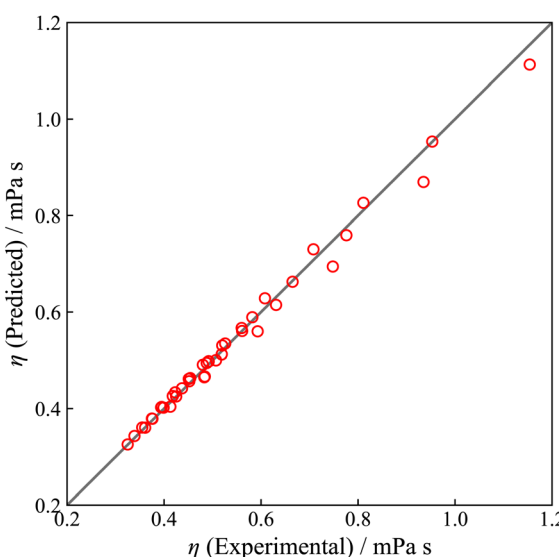


Fig. 7 Viscosity parity plot for the *n*-hexane (1) + CPME (2) + propan-1-ol (3) ternary mixture at 298.15 K and 101.325 kPa. (○): Helmholtz scaling theory. The experimental data are presented in Table 9.



Table 11 Experimental surface tensions (σ) for the *n*-hexane (1) + CPME (2) + propan-1-ol (3) ternary mixture at 298.15 K and 101.3 kPa^a

x_1	x_2	$\sigma/\text{mN m}^{-1}$	x_1	x_2	$\sigma/\text{mN m}^{-1}$
0.086	0.806	23.44	0.093	0.110	22.20
0.082	0.710	23.46	0.116	0.242	22.63
0.081	0.611	23.39	0.122	0.375	23.00
0.085	0.513	22.87	0.128	0.453	23.49
0.089	0.413	22.92	0.127	0.632	23.15
0.088	0.302	22.57	0.199	0.504	22.27
0.301	0.219	20.71	0.206	0.417	22.06
0.162	0.076	21.32	0.332	0.158	19.25
0.278	0.073	20.45	0.384	0.291	22.06
0.249	0.219	21.13	0.393	0.369	20.13
0.236	0.356	22.22	0.406	0.445	20.86
0.226	0.471	22.68	0.525	0.286	19.52
0.210	0.592	23.06	0.547	0.185	19.13
0.182	0.709	23.55	0.559	0.099	18.71
0.175	0.782	23.84	0.085	0.805	23.89
0.335	0.592	22.24	0.085	0.711	23.77
0.327	0.456	21.99	0.091	0.615	23.75
0.306	0.317	21.74	0.090	0.511	23.36
0.252	0.154	21.41	0.091	0.391	23.04
0.265	0.083	20.85	0.097	0.296	22.84
0.280	0.020	20.55	0.098	0.202	22.34
0.415	0.051	19.94	0.091	0.100	22.06
0.387	0.247	20.51	0.202	0.097	20.97
0.374	0.409	21.63	0.193	0.195	21.38
0.369	0.527	21.75	0.179	0.321	22.02
0.366	0.594	22.00	0.424	0.496	20.91
0.531	0.401	20.57	0.427	0.401	20.57
0.542	0.223	20.13	0.428	0.303	20.53
0.498	0.079	19.65	0.432	0.200	20.23
0.490	0.004	19.32	0.427	0.103	20.02
0.683	0.075	18.99	0.482	0.219	19.51
0.570	0.359	20.36	0.481	0.319	19.99
0.560	0.410	20.29	0.471	0.425	20.39
0.745	0.166	18.89	0.620	0.306	19.74
0.685	0.003	18.55	0.615	0.194	19.31
0.869	0.113	18.62	0.610	0.081	18.69
0.819	0.174	18.97	0.695	0.169	18.82
0.854	0.026	18.25	0.821	0.101	18.56
0.095	0.207	22.59	0.945	0.031	18.20

^a x_i represents the mole fractions of component i , σ is the surface tension. The standard uncertainties, u , are: $u(P) = 1 \text{ kPa}$, $u(T) = 0.01 \text{ K}$, and $u(x_i) = 0.001$. The combined expanded uncertainty, U_c , with a 95% confidence level ($k = 2$): $U_c(\sigma) = 0.1 \text{ mN m}^{-1}$.

mixture at 298.15 kPa and 101.3 kPa are summarized in Table 11. Considering the theoretical section, the surface tensions of the ternary mixture are fully predicted by using the SGT coupled with the SAFT-VR Mie EoS. As it was described before, this approach only uses the pure parameters (the influence parameters, c_{ii}) and the binary parameters (β_{ij}). Specifically, c_{ii} parameters were calculated by fitting the SGT theory coupled with SAFT-VR Mie EoS for pure fluids as a function of temperature (see eqn (22)). The corresponding values of c_{ii} and their average of the absolute percentage deviations are summarized in Table 12, where it is possible to observe the good fitting of the surface tension of pure fluids as a function of temperature.

For the case of surface tensions of the binary mixtures, the SGT parameters, β_{ij} , were fitted in the whole liquid mole fraction at 298.15 K and 101.3 kPa. For the case of CPME binary

Table 12 Influence parameters, c_{ii} , for SGT

Fluid	$10^{19} \times c_{ii}/\text{J mol m}^{-5}$	% $\Delta\sigma^a$
CPME ^b	3.5162	0.69
<i>n</i> -Hexane ^b	3.5815	0.29
Propan-1-ol ^c	0.8666	1.30

^a % $\Delta\sigma = (100/N_d) \sum_{i=1}^{N_d} |\sigma_i^{\text{exp}} - \sigma_i^{\text{cal}}| / \sigma_i^{\text{exp}}$. The values are fitted from experimental data. ^b Mejía and Cartes.³¹ ^c The NIST database.⁵⁶

Table 13 SGT binary interaction parameters, β_{ij}

Mixtures	β_{ij}	% $\Delta\sigma^a$
<i>n</i> -Hexane (1) + CPME (2) ^b	0.0000	1.94
<i>n</i> -Hexane (1) + propan-1-ol (3) ^c	0.0927	4.77
CPME (2) + propan-1-ol (3) ^d	0.0583	4.21

^a % $\Delta\sigma = (100/N_d) \sum_{i=1}^{N_d} |\sigma_i^{\text{exp}} - \sigma_i^{\text{cal}}| / \sigma_i^{\text{exp}}$. The values are fitted from experimental data. ^b Mejía *et al.*³² ^c Papaioannou *et al.*⁶¹ ^d Mejía *et al.*³⁴

mixtures (*i.e.*, *n*-hexane (1) + CPME (2) and CPME (2) + propan-1-ol (3)), the experimental determinations were taken from our previous studies,^{32,34} while the experimental surface tension data for *n*-hexane (1) + propan-1-ol (3) were taken from Papaioannou *et al.*,⁶¹ The numerical values of β_{ij} and the corresponding deviations are summarized in Table 13.

From Table 13, it can be seen that the theoretical approach successfully correlates the surface tension of the sub-binary mixtures that form the ternary mixture with low deviation (<5%).

In order to compare the performance of the theoretical approach for the ternary mixture, Fig. 9 illustrates the corresponding parity plot, where the SGT + SAFT-VR Mie EoS approach reproduces the experimental values with a very low deviation of 1.52%.

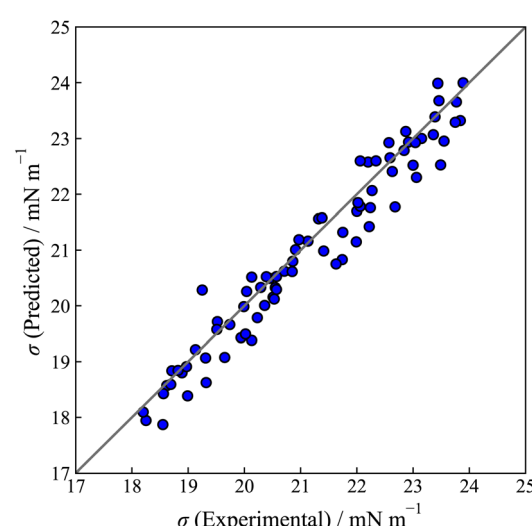


Fig. 9 Surface tension parity plot for the *n*-hexane (1) + CPME (2) + propan-1-ol (3) ternary mixture at 298.15 K and 101.30 kPa.



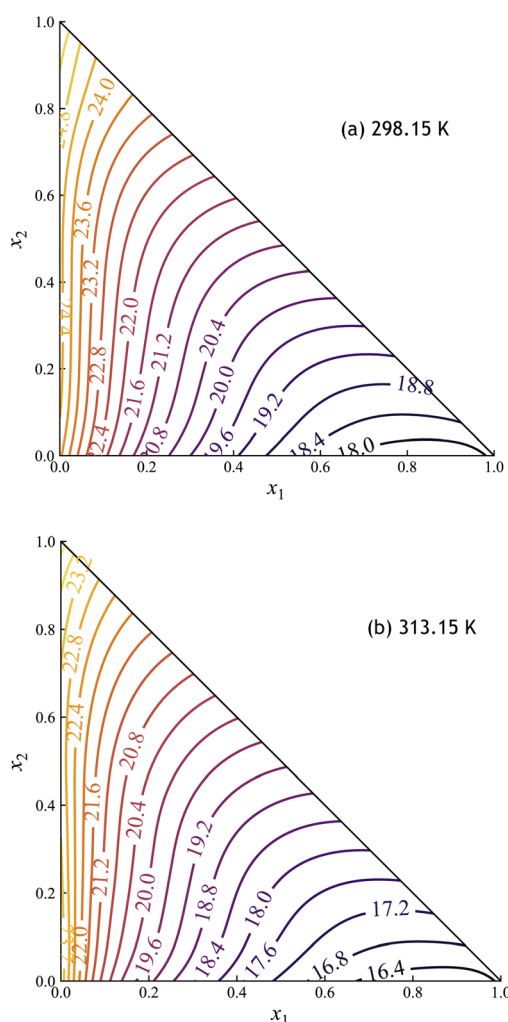


Fig. 10 Contour plot of the surface tensions (σ in mN m^{-1}) for the hexane (1) + CPME (2) + propan-1-ol (3) ternary mixture at 298.15 K and 101.30 kPa.

Additionally, Fig. 10 displays the predicted contour plot of the surface tension of the ternary mixture, σ , as a function of the liquid mole fractions, x_1 and x_2 at 101.3 kPa and two isothermal conditions, 298.15 K and 313.15 K where it is possible to observe the variation of the surface tension in the whole liquid mole fraction range under two isothermal conditions.

Complementarily, to predict the surface tensions of the mixture, the SGT + SAFT-VR Mie EoS approach provides a route to evaluate other interfacial properties, such as the interfacial concentration of components along the interfacial region, $\rho_i(z)$. $\rho_i(z)$ permits the evaluation of the absolute adsorption or surface activity of components in the interfacial region. As an illustration, Fig. 11 shows the interfacial concentration of *n*-hexane, CPME, and propan-1-ol at three different compositions: (a) *n*-hexane-rich mixture ($x_1 = 0.8$), (b) medium *n*-hexane composition ($x_1 = 0.4$), and (c) *n*-hexane-poor region ($x_1 = 0.1$).

From Fig. 11, it is possible to observe that CPME does not exhibit adsorption under the conditions studied. *n*-hexane and propan-1-ol display positive surface activity or adsorption (*i.e.*, $d\rho_i/dz = 0$; $d^2\rho_i/dz^2 < 0$). Specifically, at high and medium *n*-hexane concentrations, the propan-1-ol is adsorbed in the interfacial region, whereas *n*-hexane is adsorbed when its mole fractions are low. Adsorption is directly influenced by equilibrium conditions and the components that form the mixtures. In mixtures of dissimilar molecules, the component with the lowest intrinsic free energy and surface tension preferentially adsorbs at the interface, resulting in reduced interfacial free energy and surface tension.^{30,62} The results demonstrate that the SGT combined with the SAFT-VR Mie EoS accurately describes the interfacial properties of the ternary system, enabling precise predictions of surface tension and density profiles across the interface.

All interfacial properties reported in this section (*i.e.*, parity and contour surface tension plots of the surface tension and interfacial profiles) for the ternary mixture at 298.15 K and 101.30 kPa can be reproduced using The Jupyter-Notebook “Interfacial Properties.ipynb” which is available as an open-source on our GitHub repository.⁵⁹

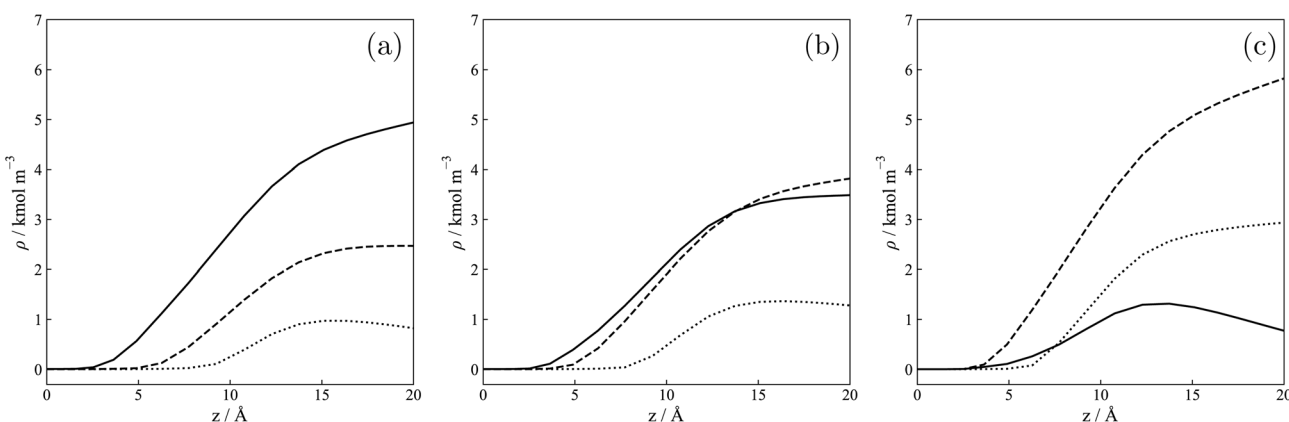


Fig. 11 Concentration interfacial profiles $\rho_i(z)$ across the vapor–liquid phases. —: *n*-hexane; - - -: CPME; ···: propan-1-ol. (a) High *n*-hexane composition, (b) medium *n*-hexane composition, and (c) low *n*-hexane composition.

5 Conclusion

Current environmental regulations and the need to use eco-friendly and renewable fuels for transportation have impulsed the evaluation of new oxygenated additives for fossil fuels. The new oxygenates provide several advantages, such as the enhancement of the oxygen excess to reduce the unburned, increase in the octane-ratio, and decrease of the fossil fuel dependence. Traditionally, oxygenated gasoline is formed as a blend of hydrocarbons, alcohols, and ethers or esters, where, nowadays, the latter three are impulsed to be produced from renewable sources. In this work, a new potential oxygenated mixture is explored from the thermophysical point of view. Specifically, this work reports the phase equilibria, liquid mass densities, liquid viscosities, and surface tensions for the *n*-hexane + CPME + propan-1-ol ternary mixture. The approach used here combines both direct experimental measurements and full predictive theoretical modeling. Considering the results, it is possible to conclude that the explored ternary mixture displays an isobaric vapor-liquid phase equilibrium that positively deviates from Raoult's law, showing zeotropic behavior. For other explored thermophysical properties (*i.e.*, liquid mass density, surface tension, and liquid viscosity), it was observed that these three properties negatively deviate under the corresponding linear or ideal behavior, and no ternary stationary points were detected under the analyzed conditions (*i.e.*, 298.15 K and 101.3 kPa). The phase, transport, and interfacial properties of the ternary mixture are fully predicted using the SAFT-VR Mie coupled with the A-scaling and the SGT theories, reporting very low deviations. In addition to the comparison between experimental determinations and theoretical predictions, the theoretical methodology used here provides a route not only to continuous interpolate predictions but also to explore unmeasurable properties, such as the interfacial concentrations along the interfacial region. In the latter case, it was possible to conclude that CPME does not display surface activity, whereas both *n*-hexane and propan-1-ol display positive surface activity (or absolute adsorption) along the interfacial region, and its magnitude changes with the equilibrium conditions.

Data availability

All the numerical and graphical results reported in this work can be reproduced by using the Jupyter notebooks: "Vapor Liquid Equilibria.ipynb", "Liquid viscosities - Scaling theory.ipynb" and "Interfacial Properties.ipynb" which are available as an open source on our GitHub repository.⁵⁹

Author contributions

Isaías Huenuvil-Pacheco: conceptualization (equal), writing – original draft (lead), software (lead), investigation (equal), formal analysis (equal). Marcela Cartes: conceptualization (equal), investigation (equal), experimental determinations (lead), methodology (equal), formal analysis (equal), validation (equal), data curation (lead), writing – review & editing (equal).

Andrés Mejía: conceptualization (equal), investigation (equal), methodology (equal), formal analysis (equal), validation (equal), writing – review & editing (equal), funding acquisition (lead).

Conflicts of interest

The authors declare no competing financial interest.

Acknowledgements

This work was financed by the Chilean National Agency for Research and Development (Agencia Nacional de Investigación y Desarrollo de Chile, ANID) under the grant Project FONDECYT Project 1230654. I. H.-P. acknowledges the financial support from ANID – Subdirección de Capital Humano, Beca Doctorado Nacional/2022-21222234.

Notes and references

- 1 P. Laha and B. Chakraborty, *Renew. Sustain. Energy Rev.*, 2017, **73**, 95–114.
- 2 K. Nanthagopal, B. Ashok, R. S. Garnepu, K. R. Tarun and B. Dhinesh, *Energy Conv. Manag.*, 2019, **179**, 104–113.
- 3 H. Pan, H. Li, H. Zhang, A. Wang, D. Jin and S. Yang, *Energy Conv. Manag.*, 2018, **166**, 534–544.
- 4 Y. Hua, *Fuel*, 2024, **357**, 129749.
- 5 W. Zhao, J. Yan, S. Gao, T. H. Lee and X. Li, *Fuel*, 2022, **307**, 121692.
- 6 R. Luque and J. Clark, *Handbook of Biofuels Production: Processes and Technologies*, Elsevier, Amsterdam, Netherlands, 2010.
- 7 *Handbook of fuels. Energy sources for transportation*, ed. B. Elvers and A. Schütze, Wiley-VCH, Weinheim, Germany, 2nd edn, 2022.
- 8 *Biorefinery of Alternative Resources: Targeting Green Fuels and Platform Chemicals*, ed. S. Nanda, D.-V. N. Vo and P. K. Sarangi, Springer, Singapore, 2020.
- 9 G. de Gonzalo, A. R. Alcántara and P. D. de María, *Chem. Sus. Chem.*, 2019, **12**, 2083–2097.
- 10 K. Watanabe, N. Yamagawa and Y. Torisawa, *Org. Process Res. Dev.*, 2007, **11**, 251–258.
- 11 H. Liu, Z. Wang, Y. Long and J. Wang, *Fuel*, 2015, **157**, 255–260.
- 12 A. Çakmak, M. Kapsuz and H. Özcan, *Energ. Source Part A*, 2023, **45**, 178–193.
- 13 I. Schifter, U. González and C. González-Macías, *Fuel*, 2016, **183**, 253–261.
- 14 K. F. Yee, A. R. Mohamed and S. H. Tan, *Renew. Sustain. Energy Rev.*, 2013, **22**, 604–620.
- 15 O. I. Awad, R. Mamat, T. K. Ibrahim, A. T. Hammid, I. Yusri, M. A. Hamidi, A. M. Humada and A. Yusop, *Renew. Sustain. Energy Rev.*, 2018, **91**, 394–408.
- 16 Q. Wang, J. Ni and R. Huang, *Fuel*, 2022, **309**, 122129.
- 17 L. C. D. Freitas and S. Kaneko, *Energy Econ.*, 2011, **33**, 1146–1154.



18 N. H. Kasmuri, S. Kamarudin, S. R. S. Abdullah, H. Hasan and A. M. Som, *Renew. Sustain. Energy Rev.*, 2017, **79**, 914–923.

19 E. Khalife, M. Tabatabaei, A. Demirbas and M. Aghbashlo, *Prog. Energy Combust. Sci.*, 2017, **59**, 32–78.

20 A. K. Agarwal, *Prog. Energy Combust. Sci.*, 2007, **33**, 233–271.

21 M. U. Kaisan, L. O. Yusuf, I. U. Ibrahim, S. Abubakar and S. Narayan, *ACS Omega*, 2020, **5**, 26454–26462.

22 M. K. Jamil, M. Akhtar, M. Farooq, M. M. Abbas, M. K. Saad, K. Ahmad, M. A. Kalam and A. Abdelrahman, *Energies*, 2022, **15**, 5757.

23 Y. Çelebi, M. Cengiz and H. Aydin, *J. Energy Inst.*, 2025, **120**, 102047.

24 Z. Tosun and A. Huseyin, *Clean. Eng. Technol.*, 2022, **3**, 100041.

25 Y. Qian, J. Guo, Y. Zhang, W. Tao and X. Lu, *Appl. Therm. Eng.*, 2018, **144**, 126–136.

26 P. Mello, F. Wildner, G. S. de Andrade, R. Cataluna and R. da Silva, *J. Braz. Soc. Mech. Sci. Eng.*, 2014, **36**, 403–410.

27 W. Yuan, A. Hansen and Q. Zhang, *Fuel*, 2009, **88**, 1120–1126.

28 G. Chaparro, M. Cartes and A. Mejía, *Fuel*, 2020, **279**, 118415.

29 M. Cartes, G. Chaparro, G. Alonso and A. Mejía, *J. Mol. Liq.*, 2022, **359**, 119353.

30 A. Mejía, M. Cartes, A. Velásquez, G. Chaparro and V. Sanhueza, *Fluid Phase Equilib.*, 2022, **558**, 113444.

31 A. Mejía and M. Cartes, *J. Chem. Eng. Data*, 2019, **64**, 1970–1977.

32 A. Mejía, M. Cartes and G. Chaparro, *Fluid Phase Equilib.*, 2020, **520**, 112654.

33 A. Mejía, M. Cartes and A. Velásquez, *J. Chem. Eng. Data*, 2020, **65**, 4142–4149.

34 A. Mejía, M. Cartes and A. Velásquez, *J. Chem. Thermodyn.*, 2021, **157**, 106400.

35 A. Allal, M. Moha-Ouchane and C. Boned, *Phys. Chem. Liq.*, 2001, **39**, 1–30.

36 A. Allal, C. Boned and A. Baylaucq, *Phys. Rev. E*, 2001, **64**, 011203.

37 J. van der Waals, *Z. Phys. Chem.*, 1894, **13**, 657–725.

38 J. W. Cahn and J. E. Hilliard, *J. Chem. Phys.*, 1958, **28**, 258–267.

39 H. Davis and L. Scriven, *Adv. Chem. Phys.*, 1982, **49**, 357–454.

40 B. Musthafa, B. Saravanan, M. Asokan, S. Devendiran and K. Venkatesan, *Egypt. J. Pet.*, 2023, **32**, 35–40.

41 T. Lafitte, A. Apostolakou, C. Avendaño, A. Galindo, C. S. Adjiman, E. A. Müller and G. Jackson, *J. Chem. Phys.*, 2013, **139**, 154504.

42 C. I. Goncalves, G. M. Silva, P. M. Ndiaye and F. W. Tavares, *Ind. Eng. Chem. Res.*, 2021, **60**, 9231–9245.

43 A. Mejía, M. Cartes and A. Velásquez, *J. Chem. Eng. Data*, 2021, **66**, 2783–2792.

44 H. C. V. Ness and M. M. Abbott, *Classical Thermodynamics of Nonelectrolyte Solutions*, McGraw-Hill Book Co, New York, 1982.

45 J. Wisniak, *Ind. Eng. Chem. Res.*, 1993, **32**, 1531–1533.

46 J. Wisniak and A. Tamir, *J. Chem. Eng. Data*, 1977, **22**, 253–260.

47 S. Dufal, T. L. A. J. Haslam, A. Galindo, G. N. I. Clark, C. Vega and G. Jackson, *Mol. Phys.*, 2015, **113**, 948–984.

48 S. H. Huang and M. Radosz, *Ind. Eng. Chem. Res.*, 1990, **29**, 2284–2294.

49 S. P. Tan, H. Adidharma and M. Radosz, *Ind. Eng. Chem. Res.*, 2004, **43**, 203–208.

50 M. L. Michelsen and J. M. Mollerup, *Thermodynamic Models: Fundamentals and Computational Aspect*, Tie-Line Publications, Holte, 2nd edn, 2007.

51 A. Mejía, E. A. Müller and G. C. Maldonado, *J. Chem. Inf. Model.*, 2021, **61**, 1244–1250.

52 S. Chapman and T. G. Cowling, *The Mathematical Theory of Non-uniform Gases*, Cambridge University Press, Cambridge, 3rd edn, 1991.

53 P. D. Neufeld, A. Janzen and R. Aziz, *J. Chem. Phys.*, 1972, **57**, 1100–1102.

54 C. R. Wilke, *J. Chem. Phys.*, 1950, **18**, 517–519.

55 J. Gmehling, *Azeotropic Data*, Wiley-VCH, Weinheim, 2nd edn, 2004.

56 V. Diky, R. D. Chirico, M. Frenkel, A. Bazyleva, J. W. Magee, E. Paulechka, A. Kazakov, E. W. Lemmon, C. D. Muzny, A. Y. Smolyanitsky, S. Townsend and K. Kroenlein, *Thermo Data Engine (TDE) Version 10.1 (Pure compounds, Binary mixtures, Ternary mixtures and Chemical reactions). NIST Standard Reference Database 103b. Thermodynamics Research Center (TRC), Applied Chemicals and Material Division. Standard Reference Data Program*, National Institute of Standards and Technology (NIST), 2016.

57 J. T. Cripwell, S. A. Smith, C. E. Schwarz and A. J. Burger, *Ind. Eng. Chem. Res.*, 2018, **57**, 9693–9706.

58 P. Prabhu and M. V. Winkle, *J. Chem. Eng. Data*, 1963, **8**, 210–214.

59 https://github.com/AMThermo/Biphasic_Equilibria/tree/main/Hexane%2BCPME%2BPropanol, accessed: 2025-07-3.

60 B. Orge, M. Iglesias, A. Rodriguez, J. M. Canosa and J. Tojo, *Fluid Phase Equilib.*, 1997, **133**, 213–227.

61 D. Papaaoannou and C. G. Panayiotou, *J. Chem. Eng. Data*, 1994, **39**, 457–462.

62 C. Miqueu, B. Mendiboure, C. Graciaa and J. Lachaise, *Fluid Phase Equilib.*, 2004, **218**, 189–203.

